Article

Structure

Structures of C1q-like Proteins Reveal Unique Features among the C1q/TNF Superfamily

Graphical Abstract

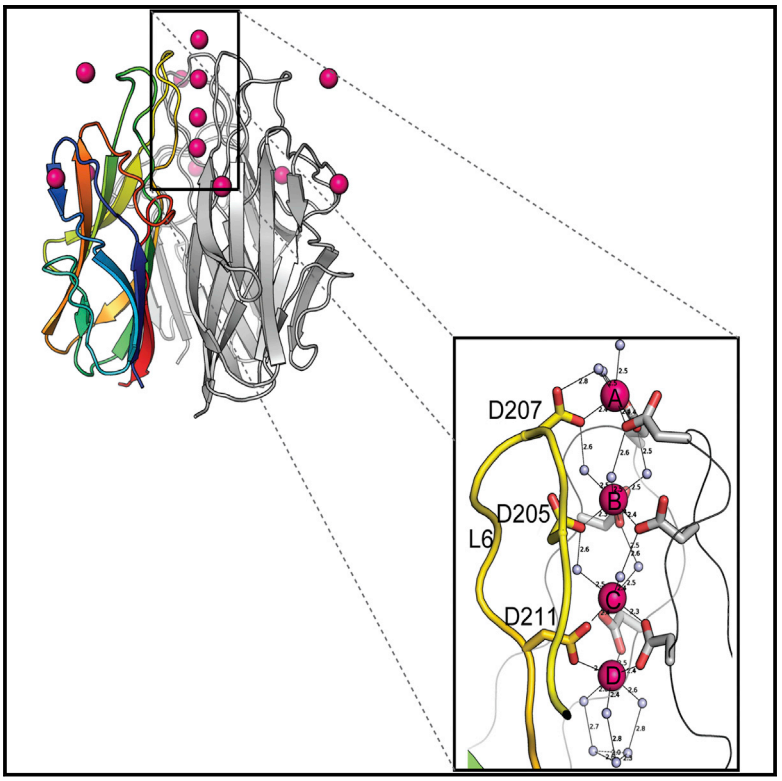

Authors

Susanne Ressl, Brandon K. Vu, ..., Thomas C. Südhof, Axel T. Brunger

Correspondence

brunger@stanford.edu (A.T.B.), suressl@indiana.edu (S.R.)

In Brief

C1q-like-1, -2, and -3 proteins bind to brain-specific angiogenesis inhibitor 3, an adhesion-type G-protein coupled receptor that may regulate dendritic morphology by organizing actin filaments. Ressl et al. report high-resolution crystal structures of the C1QL protein family. The structures reveal unique features among the C1q/TNF superfamily that are likely associated with their specific brain functions.

Highlights

- C1QL proteins structures reveal conserved electrostatic potential surface patterns
- C1QL proteins structures reveal conserved Ca^{2+} binding along the trimeric axis
- Ca^{2+} binding contributes to thermal stability of C1QL proteins

Accession Numbers

4QQ2
4QPY
4QQH
4QQL
4QQO
4QQP

Ressl et al., 2015, Structure *23*, 688–699
April 7, 2015
http://dx.doi.org/10.1016/j.str.2015.01.019

CellPress

Structure
Article

Structures of C1q-like Proteins Reveal Unique Features among the C1q/TNF Superfamily

Susanne Ressl,[1,4,*] Brandon K. Vu,[1] Sandro Vivona,[1] David C. Martinelli,[1] Thomas C. Südhof,[1,2] and Axel T. Brunger[1,2,3,*]
[1]Department of Molecular and Cellular Physiology, Stanford University, Stanford, CA 94305, USA
[2]Howard Hughes Medical Institute, Stanford, CA 94305, USA
[3]Departments of Neurology and Neurological Sciences, Photon Science, and Structural Biology, Stanford University, Stanford, CA 94305, USA
[4]Present address: Molecular and Cellular Biochemistry Department, Indiana University Bloomington, Bloomington, IN 47405, USA
*Correspondence: brunger@stanford.edu (A.T.B.), suressl@indiana.edu (S.R.)
http://dx.doi.org/10.1016/j.str.2015.01.019

SUMMARY

C1q-like (C1QL) -1, -2, and -3 proteins are encoded by homologous genes that are highly expressed in brain. C1QLs bind to brain-specific angiogenesis inhibitor 3 (BAI3), an adhesion-type G-protein coupled receptor that may regulate dendritic morphology by organizing actin filaments. To begin to understand the function of C1QLs, we determined high-resolution crystal structures of the globular C1q-domains of C1QL1, C1QL2, and C1QL3. Each structure is a trimer, with each protomer forming a jelly-roll fold consisting of 10 β strands. Moreover, C1QL trimers may assemble into higher-order oligomers similar to adiponectin and contain four Ca^{2+}-binding sites along the trimeric symmetry axis, as well as additional surface Ca^{2+}-binding sites. Mutation of Ca^{2+}-coordinating residues along the trimeric symmetry axis lowered the Ca^{2+}-binding affinity and protein stability. Our results reveal unique structural features of C1QLs among C1q/TNF superfamily proteins that may be associated with their specific brain functions.

INTRODUCTION

Brain function relies on the connectivity and correct circuitry between diverse types of neurons. Chemical synapses are specialized cell-cell junctions that establish the circuitry of the brain and connect neurons into networks. Synapses are characterized by a distinct and stable structural feature, the synaptic cleft, which connects the pre- and postsynaptic neuron via a ~20-nm gap. A series of synaptic cell-adhesion molecules spans the synaptic cleft and regulates the properties of synapses. Dysfunction of any of these elements may lead to neuropsychiatric and neurodegenerative disorders, which are increasingly being referred to as synaptopathies, highlighting the importance of understanding the structure and function of synapses in normal brain development (Südhof, 2008). Yet, despite decades of intense research, many elements of the regulation of synaptic function (and specifically of the structure and function of proteins involved therein) remain poorly understood.

Members of the C1q/TNF superfamily play a role in synapse homeostasis (Hirai et al., 2005; Matsuda and Yuzaki, 2011; Stevens et al., 2007; Uemura et al., 2010). This has been best demonstrated for cerebellins, which bind to presynaptic neurexins and postsynaptic GluRδ2 receptors, forming a transsynaptic cell-adhesion complex (Uemura et al., 2010). Moreover, complement component *1*, *q* subcomponent-like (C1QL) proteins serve as ligands for the brain-specific angiogenesis inhibitor (BAI) cell-adhesion G-protein coupled receptor (GPCR) family, and both C1QLs and BAI GPCRs are highly expressed in the CNS (Bolliger et al., 2011; Cork and Van Meir, 2011; Hamoud et al., 2014; Hochreiter-Hufford et al., 2013). BAI proteins have been linked to a number of diverse functions, including angiogenesis and engulfment of apoptotic cells (Cork and Van Meir, 2011; Stephenson et al., 2014). In addition, systematic cancer-genomics analysis identified *BAI* genes as frequently mutated in various forms of cancer (Kan et al., 2010). Furthermore, SNPs in *BAI3* significantly associate with schizophrenia and predispose to addiction in genome-wide association studies (DeRosse et al., 2008; Liu et al., 2006). Bolliger and colleagues found that all four C1QL proteins interact with BAI3, and at least C1QL3 does so in a Ca^{2+}-dependent manner (Bolliger et al., 2011). Addition of excess of C1QLs to the medium of cultured neurons decreases synapse density, suggesting that C1QLs function as synaptic regulators. However, the mechanism of C1QL action remains unclear, and understanding this mechanism requires information about the structure and function of C1QLs.

While the specific functions of C1QL proteins are still largely unknown, the differences in their expression may correlate with distinct physiological roles in the brain. *C1ql1*, *C1ql2*, and *C1ql3* are expressed almost exclusively in the CNS and found in distinct spatial regions of the brain (Iijima et al., 2010). C1QL proteins may be involved in synapse homeostasis, which includes the formation, maintenance, and/or elimination of synapses (Bolliger et al., 2011). C1QL proteins are secreted and not membrane bound; they are composed of an N-terminal signal peptide, followed by a sequence of ~15 residues with two conserved cysteines important for higher-order oligomerization (Iijima et al., 2010), a spacer region of 15–35 residues, 17 G-X-Y collagen-like repeats, and a C-terminal globular C1q domain of approximately 140 residues (Figure 1A). Although the hydrophobic core of the globular C1q domain is highly conserved (Shapiro and Scherer, 1998), each C1q domain family member harbors specific structural properties that may be related to its

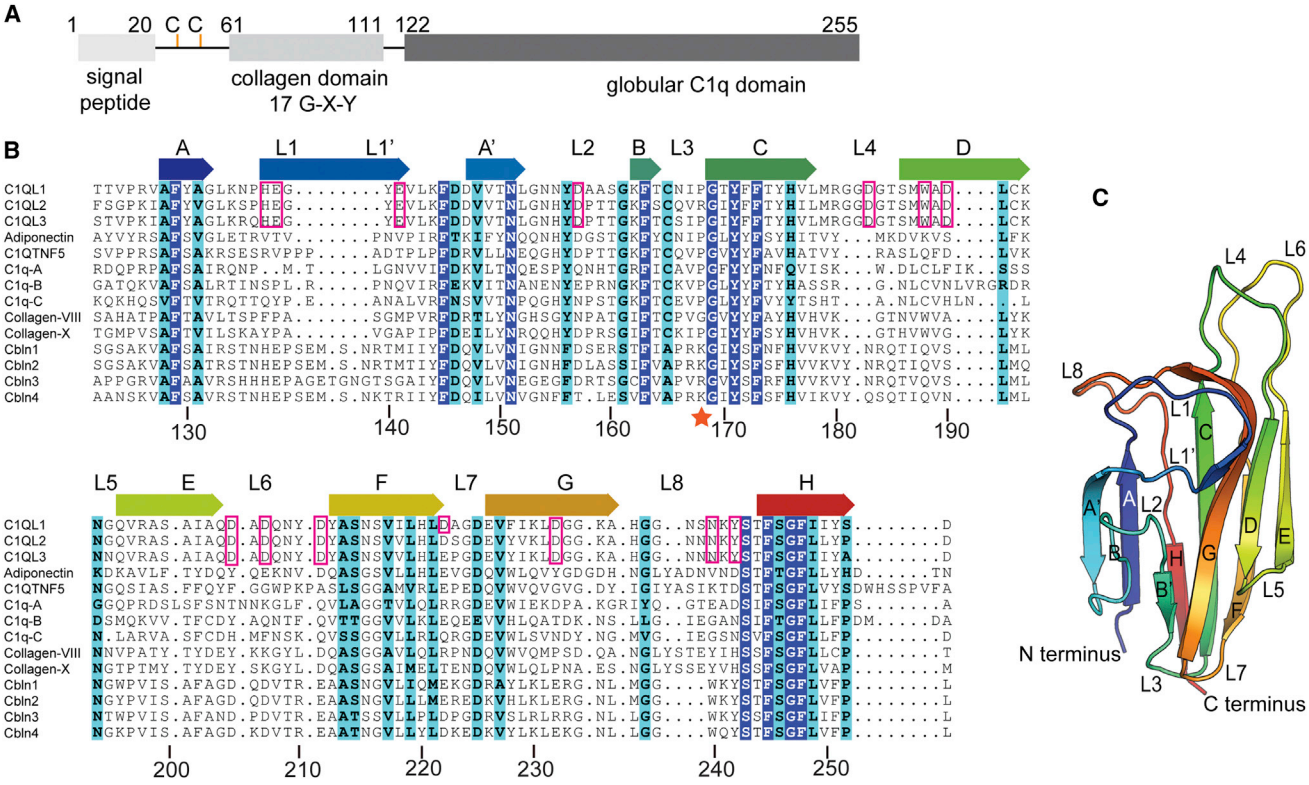

Figure 1. Sequence Alignment of the C1q/TNF Superfamily, C1QL Protein Domain Organization, and Domain Architecture of C1QL1

(A) Domain architecture of C1QL3.

(B) Sequence alignment of globular C1q domains from C1q/TNF superfamily members. Sequences are those of adiponectin, C1QTNF5, complement protein C1q, collagen VIII NC1, collagen X NC1, and Cbln1–4 (all from mice). Conserved residues are highlighted in colors ranging from blue to cyan according to their conservation, from high to low, respectively. Residues involved in cation binding are boxed in magenta. The dark orange star marks the position of arginine R168 of C1QL2.

(C) Structure of the globular C1q protomer domain of C1QL1 (cartoon representation). The protomer is arranged as a 10-strand jelly-roll fold consisting of two antiparallel stranded β strands composed of (A, A′, H, C, F) and (E, D, G, B, B′). Rainbow coloring progresses from the N terminus (blue) to the C terminus (red).

function. For example, metal binding to the globular C1q domains is not a conserved feature throughout the C1q/TNF superfamily. For those members that bind metals, metal binding is thought to have a structure-stabilizing effect (Bogin et al., 2002; Shapiro and Scherer, 1998) or, as in the case of C1QL3 and BAI3, it may mediate protein-protein interactions.

The presence of a globular C1q domain is the hallmark of the C1q/TNF superfamily, the members of which are involved in various important physiological functions, such as the innate immune response (Reid et al., 1982), insulin metabolism (Yamauchi et al., 2003), and synapse homeostasis (Bolliger et al., 2011; Matsuda et al., 2010; Uemura et al., 2010). In some cases, these functions are dependent on the formation of higher-order quaternary structures (Waki et al., 2003). In many cases, the C1q domain itself forms homo- and heterotrimers, which are essential for their function (Roumenina et al., 2005). Furthermore, different high-molecular-weight populations of adiponectin, a C1q domain protein closely related to C1QLs and cerebellins, have been observed by electron microscopy (EM) and SDS gel electrophoresis (Iijima et al., 2010; Bolliger et al., 2011) and are attributed to specific physiological functions (Hug et al., 2004; Kadowaki and Yamauchi, 2005). It is unknown if other C1q/TNF superfamily members form different populations of multimers that have distinct activities based upon the extent of their multimerization.

Here, we determined the crystal structures of the globular C1q domains of C1QL1, C1QL2, and C1QL3, all of which assemble into trimers. Electrostatic potential surface maps of the C1QL structures revealed a conserved, largely negatively charged pattern distinct from that of other globular C1q-domain proteins. Higher-order oligomers of C1QL3 were observed by size exclusion chromatography coupled to multiangle laser light scattering (SEC-MALS), and an 18-mer oligomer was modeled based on the packing of one of the crystal structures, resulting in a ring-like arrangement of six C1QL3 trimers. Remarkably, the C1QL3 18-mer model could be readily docked into an EM density map of adiponectin (Radjainia et al., 2008). Our crystal structures of C1QL1 and C1QL3 revealed C1QL-specific conserved Ca^{2+}-binding sites along the trimeric symmetry axis and on the surface of the trimer, whereas C1QL2 was crystallized in an apo state. Characterization of mutants of Ca^{2+}-coordinating residues along the trimeric symmetry axis by circular dichroism (CD) and isothermal titration calorimetry (ITC) experiments suggest that Ca^{2+} binding contributes to thermal stability of the globular

Table 1. Crystallographic Table: Data Collection and Refinement

	C1QL1	C1QL2	C1QL3	C1QL3	C1QL3 D205A	C1QL3 D207A
Crystallization conditions	0.2 M $CdCl_2$, 40% MPD, (pH 4.3), 19°C	60% Tacsimate (pH 7.0), 19°C	30% PEG 400, 0.1 M Na-acetate (pH 4.6), 0.01 M $CdCl_2$, 19°C	0.2 M magnesium acetate tetrahydrate, 0.1 M sodium cacodylate trihydrate (pH 6.5), 20% PEG 8000, 19°C	0.2 M $MgCl_2$, 0.1 M Bis-Tris (pH 5.5), 25% PEG 3350, 19°C	30% PEG 400, 0.1 M Na-acetate (pH 4.6), 0.01 M $CdCl_2$, 19°C
Beamline	SSRL BL11-1	ALS BL8.22	SSRL BL12-2	SSRL BL11-1	SSRL BL11-1	SSRL BL12-2
Space group	P212121	F432	H32	P1	H32	H32
Unit cell	a = 53.07, b = 71.41, c = 85.97	a = 225.62, b = 225.62, c = 225.62	a = 76.23, b = 76.23, c = 125.4	a = 51.59, b = 82.6, c = 86.2	a = 68.48, b = 68.48, c = 65.73	a = 76.59, b = 76.59, c = 126.21
	α = 90°, β = 90°, γ = 90°	α = 90°, β = 90°, γ = 90°	α = 90°, β = 90°, γ = 120°	α = 61.44°, β = 84.5°, γ = 74.93°	α = 90°, β = 90°, γ = 120°	α = 90°, β = 90°, γ = 120°
Resolution (Å)	38–1.8	56–2.38	38.11–1.2	49.79–2.39	34.24–2.03	46.342–2.39
Number of observations	250,500	1,614,176	741,624	50,520	15,801	71,309
Number of unique reflections	30,852	20,205	41,170	31,044	6,804	30,852
Completeness	99.7	100	93.6	65	91.55	91.2
Mean $I/\sigma I$	18.2	27.2	28.4	6.4	10.1	5.9
R_{merge} on I (%)	14.7	26	6.5	6	7.3	11.8
R_{meas} on I (%)	15.6	26.2	6.7	8.5	9.5	13.8
R_{work}/R_{free} (%)	15.3/18.7	16.7/21.6	15.3/16.7	19.4/26	14.7/16.7	22.38/25.87
Ramachandran % favored	97	93	95.5	95	89.52	92.78
Ramachandran % outliers	0.25	0.7	0.7	0.1	5.65	1.69

C1q domains of C1QL proteins. We anticipate that our C1QL crystal structures will provide a framework for future studies on how C1q/TNF proteins function at the synapse.

RESULTS

Crystal Structures of C1QL1, C1QL2, and C1QL3

We determined high-resolution crystal structures of the C1q domains of C1QL1, C1QL2, C1QL3, and of two mutants of C1QL3 (Table 1). The globular C1q domains of all three proteins form a jelly-roll architecture consisting of ten β strands (Figure 1C), and they form a trimeric quaternary structure (Figure 2A) that is typical of other members of the C1q/TNF superfamily (Figure S1) (Bogin et al., 2002; Gaboriaud et al., 2003a; Kvansakul et al., 2003; Shapiro and Scherer, 1998; Tu and Palczewski, 2012). Of these, the globular C1q domain of adiponectin (ACRP30) is most similar to that of C1QLs (Figure S1).

The core of the globular C1q domain is structurally conserved across the C1q/TNF superfamily (Figure S1; Table S1). However, there are differences in the solvent-exposed loops L1, L4, L8, and L6, suggesting that these loops may be related to the unique function(s) of each family member. These differences are also reflected in the low primary sequence identity among the C1q/TNF superfamily (Figure 1B) in these regions. For example, there are large structural differences between C1QLs and collagen VIII and collagen X in loops L1, L4, and L8: collagens contain extended β strands and helical elements in these regions (Figure S1).

We observed several electron density peaks in the C1QL1 and C1QL3 structures that represent metal binding sites. The CheckMyMetal program (Zheng et al., 2014) predicted Cd^{2+} as the best match for these sites, consistent with the presence of Cd^{2+} in the crystallization solution of both C1QL1 and C1QL3. Since the ionic radius of Cd^{2+} is within 5% of that of Ca^{2+}, we refer to the metal binding sites observed in our C1QL1 and C1QL3 structures as Ca^{2+}-binding sites, and discuss them functionally as such. C1QL2 was crystallized in 60% Tascimate without divalent cations (Table 1); moreover, no substantial electron density peaks were found that would indicate residual metals that may have been present during expression and purification. Metal binding sites in the P1 crystal form of CLQL3 and the D205A mutant of C1QL3 (both of which were crystallized in the presence of Mg^{2+} rather than Cd^{2+}) are also generically referred to as Ca^{2+}-binding sites.

Conserved Electrostatic Potential Surface of C1QL Proteins

We sought to compare the electrostatic potential surfaces of C1QL proteins with that of other C1q/TNF superfamily members in order to gain clues about potential C1QL interactions with other proteins. For each crystal structure, we calculated electrostatic charges at a physiological pH of 7.4 using the PARSE force

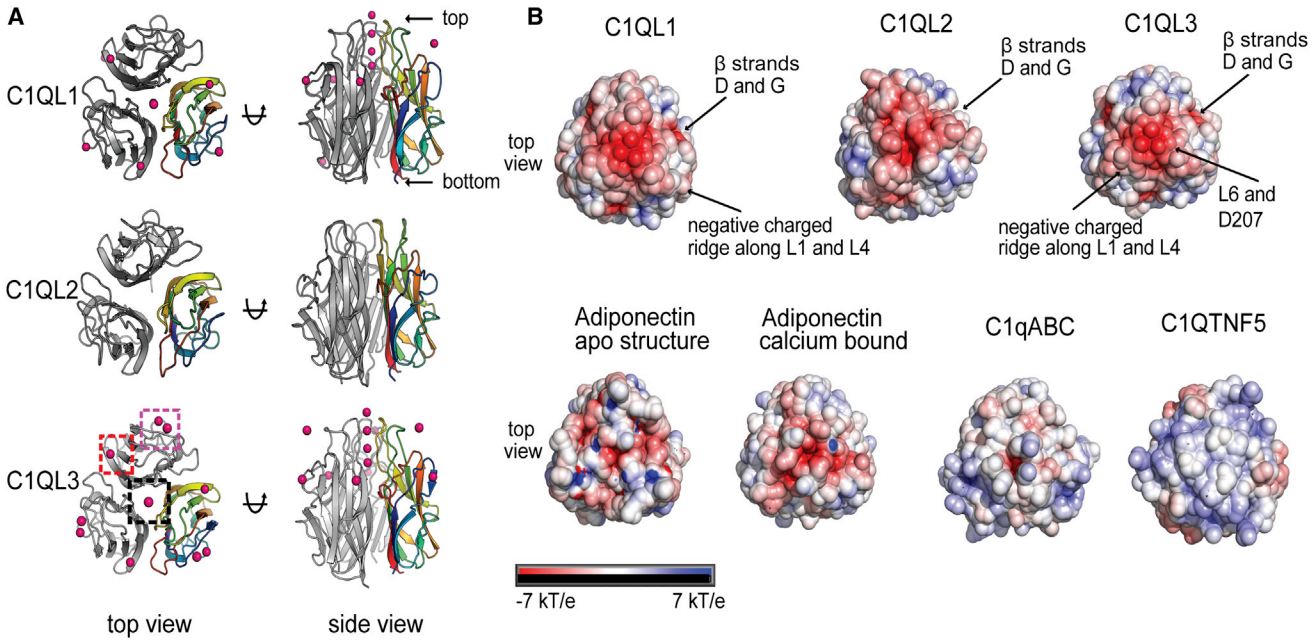

Figure 2. Crystal Structures of Globular C1q Domains of C1QL1, C1QL2 and C1QL3

(A) Crystal structures of C1QL1, C1QL2, and C1QL3 globular C1q domains are shown in two different views (cartoon representation). One of the protomers of each C1QL structure is colored using a rainbow coloring scheme from the N terminus (blue) to the C terminus (red), while the other two protomers are colored in gray. Ca^{2+} ions are colored magenta and displayed as spheres.

(B) Electrostatic potential surfaces of the C1QL1, C1QL2, and C1QL3, apo and Ca^{2+}-bound adiponectin (also referred to as Acrp30 or Adipoq, PDB ID 1c3h), immunological C1qABC (Complement System Protein C1q Chain A,B,C) (PDB ID 1pk6) (Gaboriaud et al., 2003b), and C1QTNF5 (PDB ID 4f3j) (Tu and Palczewski, 2012). All structures are displayed in the same top view as in (A). The electrostatic potential surfaces were calculated as described in the Experimental Procedures and colored according to the range –7 kT/e (red) to 7 kT/e (blue).

field (Sitkoff et al., 1994; Tang et al., 2007), which is integrated in the PDB2PQR program (Dolinsky et al., 2004), and included the charges of bound divalent cations when they were observed in the corresponding structure. The Adaptive Poisson-Boltzmann Solve (APBS) method was used to calculate the electrostatic potential surfaces (Unni et al., 2011), and the surfaces were then displayed with PyMOL (Schrödinger).

The electrostatic potential surface map of C1QL revealed a highly negatively charged pattern at the top of the C1QL trimer that is centered around the trimeric symmetry axis and extends along loops L6 and L4 toward L1 toward the perimeter of the trimer (Figure 2B). A negatively charged pocket at the perimeter of the C1QL1 and C1QL3 trimers is formed by two aspartate residues (D190 and D232) involving β strands D and G. C1QL2 is less negatively charged at this site and along L6, L4, and L1.

Compared with other globular C1q domain protein structures, such as adiponectin, C1QTNF5, and C1q, C1QL proteins have a more negative net charge (Figure 2B). Crystal structures of adiponectin trimers (PDB ID 1C3H) are available in Ca^{2+}-bound and apo states. The Ca^{2+}-bound structure of adiponectin forms a closed apex, while the Ca^{2+}-free apo structure of adiponectin forms an open apex, which is also reflected by their respective electrostatic potential surface patterns. These differences in conformation and electrostatic potential surface are reminiscent of those observed between the Ca^{2+}-bound structures of C1QL1/C1QL3 and the apo structure of C1QL2. The charge distribution of the immunological C1qABC consists of slightly negative charges near the center of the trimer surrounded by positive charges; mutational studies identified these charged residues as important for IgG and IgM binding (Kojouharova et al., 2004). In summary, the unique electrostatic potential surface pattern of the C1QL protein family differs from that of the other C1q/TNF proteins and may thus mediate their specific binding to other proteins.

Model of a C1QL3 18-mer Oligomer

Previous studies showed that C1q/TNF superfamily members form high-molecular-weight superstructures, including hexamers and larger oligomers (Bao et al., 2005; Bolliger et al., 2011; Iijima et al., 2010; Radjainia et al., 2008; Tsao et al., 2003). Specific adiponectin superstructures range in size from 6-mer to 18-mer, and distinct sizes are known to interact with different receptors at specific tissues (Hug et al., 2004; Kadowaki and Yamauchi, 2005). Moreover, several adiponectin oligomers were observed in single particle negative stain EM reconstructions at ~40 Å resolution (Radjainia et al., 2008).

We performed SEC-MALS experiments to investigate the possible existence of oligomeric states of the globular C1q domain of the C1QL3 trimer. We injected C1QL3 samples at various concentrations. We observed distinct 3-mer and 6-mer oligomeric species, along with evidence for higher-order oligomers at concentrations of 7.5 mg/ml and above (Figure 3A). Thus, C1QL3 oligomeric species are detectable by SEC-MALS despite the absence of the N-terminal collagen-stalk domain in

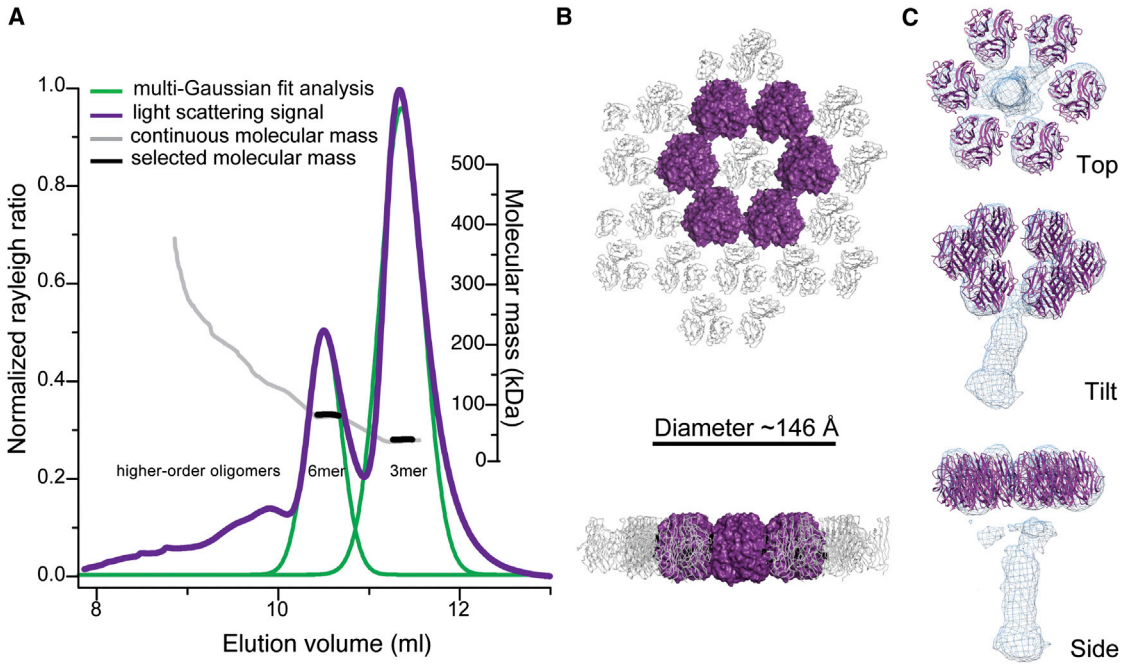

Figure 3. Oligomers of the C1QL3 Globular C1q Domain

(A) SEC-MALS experiment of C1QL3 injected at a concentration of 7.5 mg/ml. The line in purple shows the measured light scattering signal (normalized Rayleigh ratio, left *y* axis) as a function of elution volume (ml) (*x* axis). The light gray line shows the molecular mass calculated from the differential refractive index and light scattering measurements along the elution volume between 8.7 ml and 11.8 ml. The green line shows a multi-Gaussian fit analysis of the light scattering signal in the elution range between 7.5 ml and 10 ml. The black segments along the gray line indicate the fractions selected by the multi-Gaussian fit analysis, and the corresponding molecular masses (in kDa) are compatible to 3-mer, 6-mer, and higher-order oligomers.

(B) Putative C1QL3 18-mer ring produced by crystal packing in the P1 crystal form of C1QL3 at pH 6.5 (Table 1). Top view and side views showing a ring of six trimers formed by crystal packing (purple surface representation) along with the remaining nearby molecules produced by both noncrystallographic and crystallographic translational symmetry (gray cartoon representation). The specified diameter is the largest extent of the 18-mer oligomer.

(C) Docking of the C1QL3 18-mer ring (purple) into the density map of the single particle negative stain EM reconstruction of adiponectin (blue), shown in top, tilted, and side views.

our constructs, suggesting that contacts between the gC1q domains contribute to formation of higher-order oligomers.

Upon analyzing crystal packing of C1QL3 crystals grown at pH 6.5 (Table 1), we found a ring-like arrangement of six C1QL3 trimers with a diameter of ~146 Å (i.e., an 18-mer oligomer, Figure 3B; Movie S1), which is remarkably similar to the adiponectin bouquet structure (Radjainia et al., 2008). However, we note that the center of the 18-mer ring in the P1 crystal lattice is occupied with a C1QL3 trimer (Figure 3B; Movie S1) (produced by translational symmetry). To further support our model of the 18-mer C1QL ring, we docked the C1QL3 18-mer oligomer as a rigid body into the EM density map of adiponectin (Figure 3C; Movie S2). Remarkably, the planar C1QL3 18-mer ring matched the adiponectin EM density map (Figure 3C; Movie S2). We note that the globular C1q domain trimers form small contacts (~200–300 $Å^2$ as determined by PISA (Proteins, Interfaces, Structures and Assemblies; http://www.ebi.ac.uk/pdbe/pisa/) (Krissinel and Henrick, 2007). Further studies will be necessary to validate this proposed three-dimensional arrangement and functional role of a C1QL3 oligomer.

Metal Binding Sites in C1QL1 and C1QL3

The crystal structures of C1QL1 and C1QL3 revealed four Ca^{2+} ions bound along the trimeric symmetry axis involving loop L6 (Figures 4A and 5A). Additional Ca^{2+} ions were found on the surface of the trimer involving loops L1 and L4 and residues H137, E138, E141, and D183 (Figure 4B), and near β strands D and G involving aspartate residues D190 and D232 (Figure 4C; Figure S5).

Metal Binding along the Trimeric Symmetry Axis

The Ca^{2+}-binding sites along the trimeric symmetry axis of both the C1QL1 and C1QL3 structures resemble an ion channel (Figures 4A and 5A). The carboxylate groups of aspartate residues D205, D207, and D211, along with nearby water molecules, coordinate these bound Ca^{2+} ions (Figure 4A), resulting in an octahedral coordination sphere with an average metal-ligand distance of 2.5 Å (Figure S2). These Ca^{2+}-coordinating aspartate residues are conserved within the C1QL protein family across species (Figure S3). Superposition of the Ca^{2+}-bound structures of C1QL1 and C1QL3 with the apo structure of C1QL2 reveals an outward-facing conformation of the coordinating aspartate residues in the absence of Ca^{2+} (Figure 5A; Movie S3).

In order to investigate the role of Ca^{2+} binding at the trimeric symmetry axis, we mutated C1QL3 at residues predicted to affect Ca^{2+} binding along the trimeric symmetry axis (D205A, D207A, D211A) and performed structural and biophysical studies. As a consequence of the D205A mutation, divalent

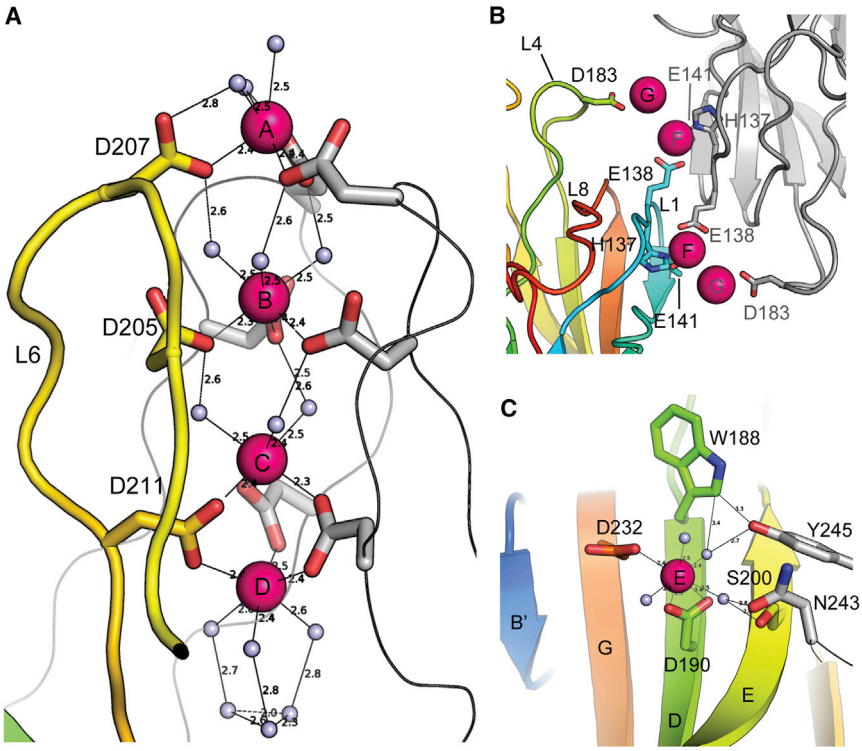

Figure 4. Ca^{2+}-Binding Sites in C1QL Proteins

(A) Ca^{2+}-binding sites along the symmetry axis of the C1QL1 trimer. Ca^{2+} ions are colored magenta, water molecules are shown as light blue-gray spheres; the corresponding binding sites in C1QL3 are similar.

(B) Ca^{2+}-binding sites involving loops L1 and L4 in the C1QL3 structure; the corresponding binding sites in C1QL1 are similar.

(C) Ca^{2+}-binding sites involving β strands D and G in the C1QL3 structure; the corresponding binding sites in C1QL1 are similar.

Ca^{2+} site A is absent in the crystal structure of the mutant (compare left panels of Figures 5A and 5B). However, the missing negative charge of that mutant is partially compensated by an inward-facing conformation of aspartate D207, thus coordinating Ca^{2+} site B (Figure 5B). Notably, loop L4 is bent toward loop L1 at the perimeter of the trimer. The crystal structure of the C1QL3 D207A mutant also revealed the absence of Ca^{2+} site A (Figure 5C), although this mutant did not lead to conformational changes of loops L4 and L6 (root-mean-square deviation is only 0.8 Å). Attempts to crystallize the C1QL3 D211A mutant failed.

To determine if Ca^{2+} binding differs at pH 4.6 and 6.5, we compared metal ion binding along the trimeric symmetric axis in C1QL3 structures crystallized at pH 4.6 and pH 6.5 (Figure S2). Both C1QL3 structures are very similar, including coordination to the metal ions (Cd^{2+} in the crystal structure at pH 4.5 and Mg^{2+} in the crystal structure at pH 6.3), suggesting that divalent cation binding is not pH sensitive in C1QL proteins.

Ca^{2+} Binding to the Trimeric Symmetry Axis Stabilizes C1QL Proteins

To test if bound Ca^{2+} ions contribute to the stability of C1QL proteins, we performed CD and ITC analysis of the D205A, D207A, D211A mutants of C1QL3 (Figure 4A). We also tested mutants that may affect Ca^{2+} binding at the peripheral Ca^{2+}-binding sites (H137A, E138A, E141A, R180A, D183A, D190A, and D232A) (Figures 4B and 4C). Wild-type and mutant proteins produced CD spectra typical for proteins that mostly consist of β strand secondary structure elements, consistent with our crystal structures (Figure 6A). We determined the melting temperature in the presence of 2 mM $CaCl_2$ for both wild-type and mutant C1QLs by measuring ellipticity at 218 nm versus temperature. Wild-type C1QL proteins are very thermally stable, as no unfolding was observed up to 100°C (Figure 6B top). In contrast, C1QL3 wild-type samples that were previously dialyzed with 5 mM EDTA unfolded at 62°C, showing that thermal stability is dependent on the presence of Ca^{2+} (Figure 6B top). The mutants of C1QL3 along the trimeric symmetry axis D207A, D211A, S214A, and D205A unfolded at 81.5°C, 84°C, 80.5°C, and 88.5°C, respectively (Figure 6B bottom). The single point mutations H137A, E138A, E141A, R180A, D183A at the perimeter of the trimer did not affect thermal stability, whereas the single point mutations D190A and D232A at β strands D and G unfolded at 70°C and 75°C, respectively (Figure 6B).

To determine the affinity of Ca^{2+} to C1QL proteins, we titrated $CaCl_2$ to the C1QL proteins that were previously depleted of ions by adding EDTA and Chelex beads to the purification buffer and then monitored Ca^{2+} binding by ITC. The binding affinity for Ca^{2+} did not differ significantly among C1QL1, C1QL2, and C1QL3, with dissociation constants (K_D) of 13.8 nM, 13.6 nM, and 11.2 nM, respectively (Figure 6C, upper panels). We note that C1QL2 exhibited a nearly identical affinity for Ca^{2+}-ions to that observed for C1QL1 and C1QL3. Since C1QL2 harbors negatively charged aspartate residues in loop L6, it is likely that Ca^{2+}-ions bind along the C1QL2 trimeric symmetry axis similarly to C1QL1 and C1QL3.

The Ca^{2+}-binding affinity decreased substantially for mutants of C1QL3 that coordinate the four Ca^{2+} ions along the trimeric symmetry axis, i.e., D205A, D207A, and D211A, with dissociation constants (K_D), of 33.1 nM, 24 nM, and 19.6 nM, respectively (Figure 6C, bottom). In contrast, single point mutations at the perimeter of C1QL3 did not change the Ca^{2+}-binding affinity (Figure S4). Collectively, these results suggest that all C1QL proteins bind Ca^{2+} ions along the trimeric symmetry axis and contribute to the thermal stability of C1QL proteins.

Differences between apo and Ca^{2+}-Bound C1QL Structures

In contrast to C1QL1 and C1QL3, the C1QL2 structure showed electron density neither at the trimeric symmetry axis nor at the perimeter of the trimer, suggesting the absence of bound ions (Figures 2A and 5A). We note that we were unable to obtain

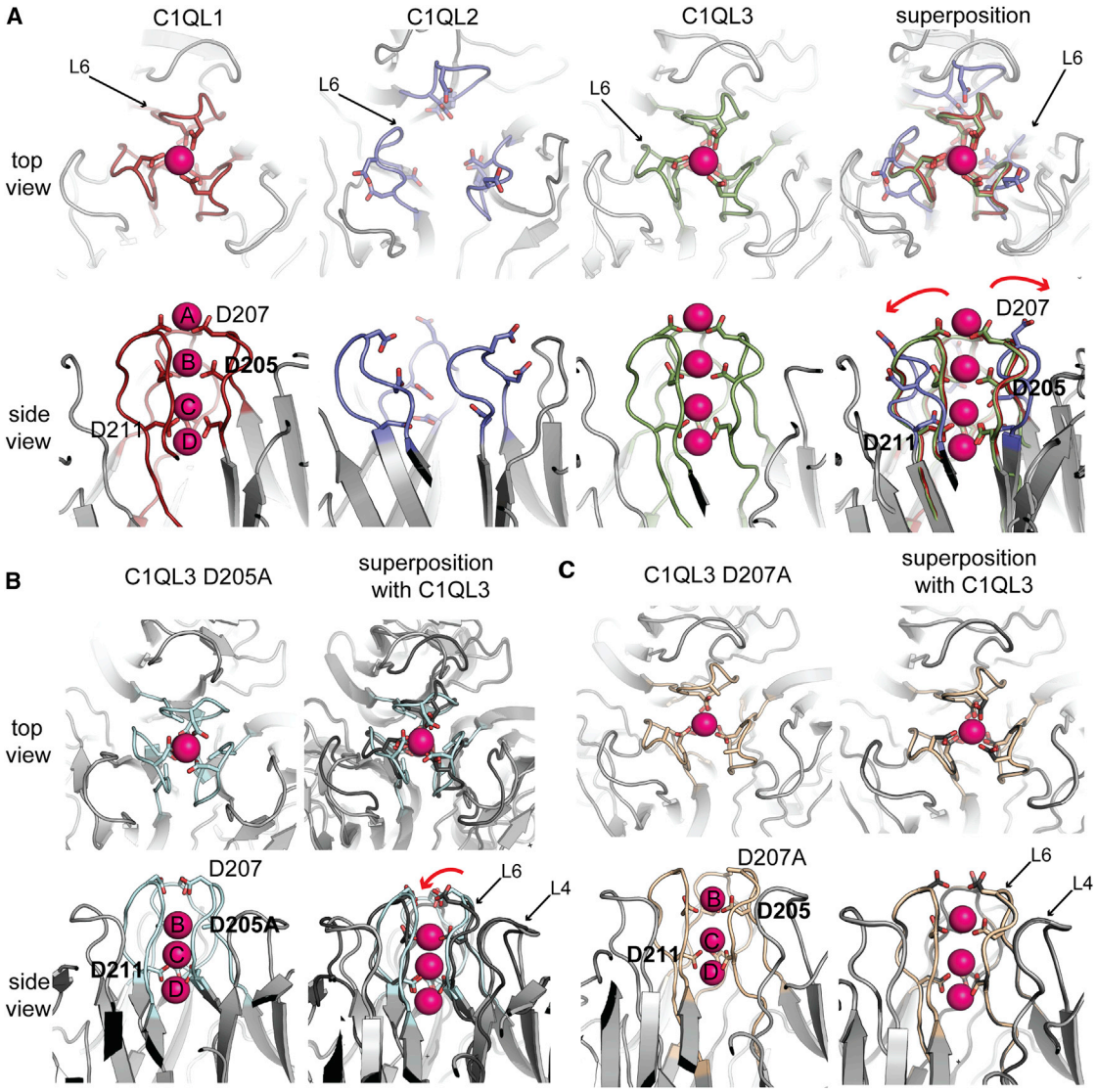

Figure 5. Ca^{2+} Binding along the Trimeric Symmetry Axis of C1QL

(A) Ca^{2+}-binding sites along the trimeric symmetry axis of C1QL1 and C1QL3. For comparison, the apo structure of C1QL2 is also shown. Two views are provided for each of the three structures: down the symmetry axis and along the side. L6 of C1QL1 is colored red, L6 of C1QL2 is colored purple, and L6 of C1QL3 is colored green. The Ca^{2+} ion A is coordinated by D207, Ca^{2+} ion B is coordinated by D205, and Ca^{2+} ions C and D are coordinated by D211. The superposition of all three structures is shown in the far right. The red arrows in the side view of the superposition indicate the conformational change of aspartate residue D207 in the apo structure of C1QL2, resulting in an opening of the C1QL2 trimer.

(B) Ca^{2+} binding along the trimeric symmetry axis of the C1QL3 mutant D205A. In the left panel, C1QL3 D205A is colored light gray and loop L6 colored light blue. The right panel shows the superposition with the C1QL3 wild-type structure (dark gray). Both C1QL3 D205A alone and in superposition with C1QL3 are the same views as in panel A. Ca^{2+} ions are colored magenta. The superposition shows the Ca^{2+} ions bound to C1QL3 D205A. Ca^{2+} ion A is missing in the C1QL3 D205A structure.

(C) Metal binding along the trimeric symmetry axis of the mutant D207A of C1QL3. In the left panel, the C1QL3 D207A structure is colored light gray and loop L6 is colored light brown. The right panel shows the superposition with the C1QL3 wild-type structure (colored dark gray). Both C1QL3 D207A alone and in superposition with C1QL3 are the same views as in (A). Ca^{2+} ions are shown as magenta spheres. The superposition shows the Ca^{2+} ions bound to C1QL3 D207A; note that Ca^{2+} ion A is missing in the C1QL3 D207A structure.

crystals of C1QL2 in similar conditions (i.e., in the presence of divalent cations) to those used for C1QL1 and C1QL3. The absence of Ca^{2+} binding in the C1QL2 structure results in an outward conformation of loop L6 as compared with C1QL1 and C1QL3 (Figure 5A; Figure S1; Movie S3).

DISCUSSION

C1q domain-containing proteins of the C1q/TNF superfamily sparked interest in neuroscience after crucial functions in synapse homeostasis were discovered for some members of the

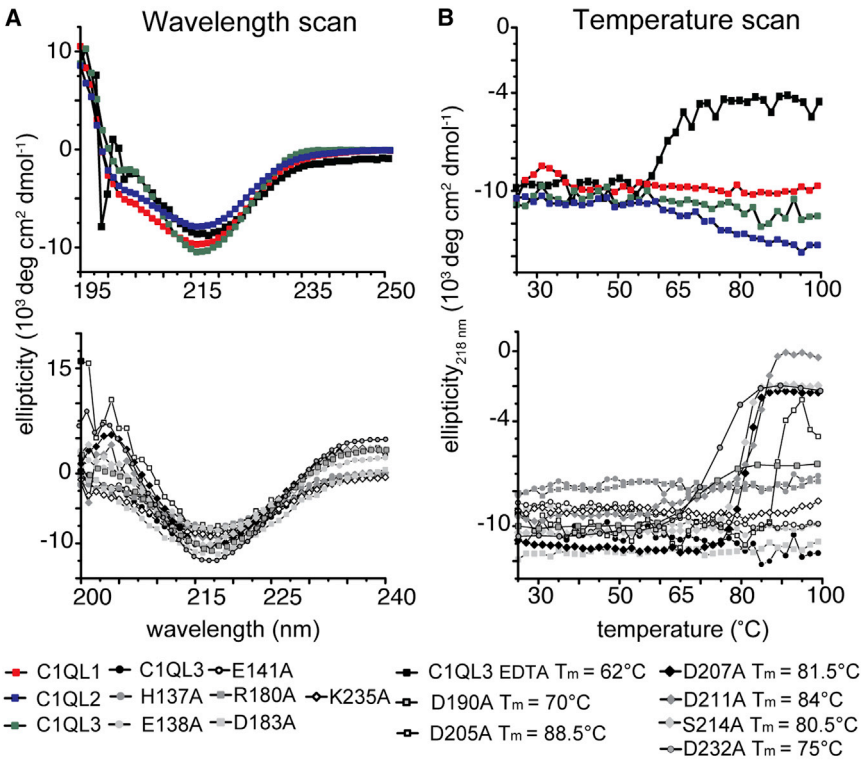

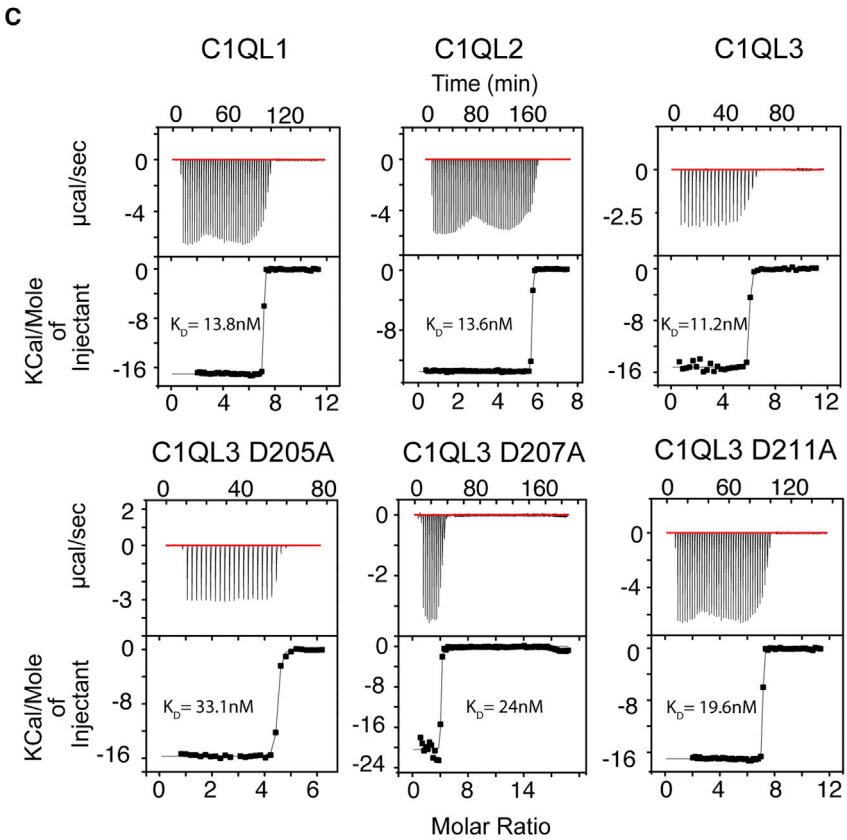

Figure 6. Thermal Stability and Ca^{2+} Affinity of C1q Domains of C1QL Proteins

(A) CD wavelength scans (195–250 nm) of C1QL1 (red), C1QL2 (blue), C1QL3 (green), and C1QL3 after dialysis in buffer containing 5 mM EDTA (black).

(B) The thermal stability was determined by monitoring ellipticity at 218 nm as a function of temperature in the 25°C–100°C range. Calculated melting temperatures (T_m) are given in degrees centigrade.

(C) Ca^{2+} affinities of C1QL proteins and specified mutants as measured by ITC. Each ITC experiment shows the recorded heat in µcal/s for each injection over the entire range of the titration experiment (top panels). The line in the corresponding bottom panels shows the nonlinear regression fit of all data points using a single set of binding site model.

superfamily, such as the complement protein C1q, cerebellins, and C1QL proteins (Hirai et al., 2005; Stevens et al., 2007). C1QL proteins are expressed highly in brain and bind to BAI3 (Bolliger et al., 2011; Iijima et al., 2010). This newly found interaction foresees a crucial role for C1QL proteins in synapse homeostasis and an indirect association with schizophrenia. In this study, we present crystal structures of the globular C1q domain of C1QL1, C1QL2, and C1QL3. In comparison with other globular C1q domain protein structures, we found unique structural features that may shape C1QL proteins unique functions.

Higher-Molecular-Weight Superstructures in C1Q/TNF Superfamily

Proteins from the C1q/TNF family form high-molecular-weight superstructures (Radjainia et al., 2008). In particular, the collagen-like stalk region together with conserved cysteine residues facilitate the formation of higher-order assemblies (Iijima et al., 2010; Radjainia et al., 2008; Tsao et al., 2003). Higher-order oligomers of adiponectin interact with distinct receptors in specific tissues (Hug et al., 2004; Kadowaki and Yamauchi, 2005). A single particle negative stain EM reconstruction of adiponectin revealed an 18-mer superstructure involving six globular C1q domains in a ring-like arrangement (Radjainia et al., 2008). Moreover, superstructures of the C1QL protein family higher than hexamer were observed by SDS gel electrophoresis (Bolliger et al., 2011; Iijima et al., 2010). Within the C1q/TNF superfamily, superstructure formation is mostly attributed to the N-terminally located conserved cysteine residues and the collagen-stalk region. However, the trimerization domain of collagens, which is distantly related to the globular C1q domain, may also drive specific superstructure formation of collagens (Boudko et al., 2009; Wirz et al., 2011). Knowing that C1QL proteins also form higher-molecular-weight oligomers, we characterized the globular C1q domain of C1QLs by SEC-MALS and observed oligomers including higher-order oligomers (Figure 3A). Using the packing of C1QL3 trimers in the P1 crystal form (Table 1), we modeled a ring of six C1QL3 trimers. By docking this 18-mer C1QL3 model into the adiponectin EM density map, we obtained a model of the C1QL3 18-mer oligomer (Figure 3C; Movie S2). Our model suggests that the globular C1q domain of C1QL proteins are in contact with each other; these contacts may stabilize the conformation of the 18-mer oligomer that is formed by the collagen domain.

Metal Binding Sites Promote Protein Stability

The structures of C1QL1 and C1QL3 revealed four Ca^{2+}-binding sites along the trimeric symmetry axis and several additional Ca^{2+}-binding sites on the surface of the trimer (Figures 2A and 4; Figure S5). The surface Ca^{2+}-binding sites are candidates for interfaces between C1QL protein and other proteins, especially in light of the Ca^{2+}-dependent binding of C1QL3 to BAI3 (Bolliger et al., 2011). CD experiments revealed that Ca^{2+} binding increases C1QL thermal stability (Figure 6B).

In contrast to C1QL1 and C1QL3, the C1QL2 structure showed no bound ions (Figures 2A and 5A). Consistent with the absence of bound ions, C1QL2 showed a wider opening of the trimer apex, mostly due to an outward conformation of L6 as compared with the conformation it forms in C1QL1 and C1QL3 (Figures 2A and 5A; Movie S3). However, we measured a similar Ca^{2+}-binding affinity for C1QL2 to that for C1QL1 and C1QL3, showing that it binds Ca^{2+} ions in solution. We suggest that the C1QL2 structure is representative for apo C1QL structures in general and that the structure of Ca^{2+}-bound C1QL2 would be similar to those of C1QL1 and C1QL3. It is unlikely that apo C1QL could exist at the synapse, considering the relatively high Ca^{2+} concentration in the synaptic cleft and the high affinity (K_D ~10 nM) of Ca^{2+} to the sites along the trimeric symmetry axis. However, it is possible that under high neuronal activity (Rusakov and Fine, 2003) Ca^{2+} concentration would be lowered in the synaptic cleft and some of the weaker Ca^{2+} binding sites on the surface of the gC1q domain trimer may be depleted, potentially affecting interactions with other factors in a Ca^{2+}-dependent fashion.

In comparison with C1QL1 and C1QL3, collagen X has three Ca^{2+} ions buried at the top quarter of the trimeric symmetry axis (Figure S1). The same type of coordination and location of three Ca^{2+} ions is also found in the adiponectin structure (PDB ID 1C3H, chain E). In both structures, all three chains contribute one aspartate residue to the coordination of three Ca^{2+} ions, in a similar fashion to the coordination of Ca^{2+} site A in C1QL1 and 3 (Figure 5A). The immunological C1qABC contains one Ca^{2+} at the very top of the trimer exposed to the solvent coordinated by glutamine Q177 from chain A, aspartate D172 and Q177 from chain B, while chain C is not involved in Ca^{2+} coordination (Gaboriaud et al., 2003b; Roumenina et al., 2005). Ca^{2+} ions along the trimeric symmetry axis have a mostly stabilizing effect on the globular C1q domain and ultimately on the N-terminal collagen domain of collagen X and adiponectin (Bogin et al., 2002; Waki et al., 2003). In contrast, the Ca^{2+} ion at the trimeric symmetry axis of immunological C1qABC plays a crucial role in ligand recognition to its various binding partners (Roumenina et al., 2005).

Our crystal structures of the C1QL1, C1QL2, C1QL3 proteins reveal unique structural features of the C1QL protein family that provide an important framework for future structural and functional studies of their role in brain development and function. Two recent publications showed the important role of the interaction between C1QL1 and BAI3 in the cerebellum. Kakewaga and colleagues showed that C1QL1 binds to BAI3 at climbing fiber-Purkinje cell synapses and that this interaction is required to determine and maintain the winner climbing fibers and is essential to mediate certain types of motor learning (Kakegawa et al., 2015). Sigoillot and colleagues showed that BAI3 promotes spinogenesis and excitatory synaptogenesis on Purkinje cells and C1QL1 controls climbing fiber synaptogenesis (Sigoillot et al., 2015). These studies highlight the emerging importance of C1QL1 and BAI3 proteins in fundamental processes in brain physiology.

EXPERIMENTAL PROCEDURES

This study is based on the glutathione *S*-transferase (GST)-fusion constructs of the globular domains of C1QL1, C1QL2, and C1QL3 described by Bolliger et al. (2011). We refer to the respective globular domains simply as C1QL1, C1QL2, and C1QL3 throughout this work. Wild-type protein refers to the unaltered sequence of the globular C1q domain of the respective C1QL protein subfamily and full-length refers to C1QL protein including the N-terminal collagen domain.

Protein Expression and Purification

All constructs included an HA tag sequence after the thrombin cleavage site and before the C1QL1, C1QL2, and C1QL3 sequence. To facilitate crystal growth of the C1QL proteins, the HA tag was removed from the original constructs (Bolliger et al., 2011). Verified by DNA sequencing, the recombinant plasmid construct of the globular C1q domains of C1QL1, C1QL2, and C1QL3 and selected single-site mutants were transformed into BL21(DE3) *Escherichia coli* cells (Invitrogen, Thermo Fisher Scientific), expressed by growing the cells to OD_{600} of 0.5 at 37°C then induced at 21°C for 12–16 hr with 0.1 mM isopropyl β-D-1-thiogalactopyranoside. Cells from 2 l of induced culture were harvested and suspended in 50 ml of PBS (pH 7.4), supplemented with PMSF to 1 mM, and 1 EDTA free Complete Protease Inhibitor Cocktail tablets (Roche). Cells were lysed by three passes through the Emulsiflex C5 homogenizer (Avestin) at 15,000 psi. Cell debris and inclusion bodies were removed by centrifugation at 4,200 rpm for 20 min. The supernatant was further centrifuged at 40,000 rpm for 25 min in a Ti45 rotor (Beckman Coulter). The supernatant GST-fusion C1QL proteins were affinity purified using glutathione Sepharose beads (GE Healthcare) in batch mode. Bound C1QL proteins were cleaved by thrombin and eluted from the column by moderate centrifugation. Eluted protein was further purified in PBS buffer by gel filtration chromatography on a Superdex 200 or Superose 6 10/300 GL column (GE Healthcare). Separate peak fractions containing C1QL1, C1QL2, and C1QL3 were pooled and if necessary for subsequent experiments, concentrated with 10k Amicon ultracentrifugal filters (EMD Millipore, Merck). The purified protein migrated on a precast AnykD gel (Bio-Rad Laboratories) as a single band with an approximate molecular mass 15 kDa, which corresponded to the expected molecular weight of the C1QL globular C1q protomer.

CD Spectroscopy

CD measurements were performed on a CD spectrometer Model 202-01 (Aviv Biomedical) equipped with a temperature controller. CD scans were performed with 12- to 24-μM samples of wild-type and mutant C1QL proteins constructs in 25% PBS-$CaCl_2$buffer (PBS: 10 mM Na_2HPO_4, 137 mM NaCl, 2.7 mM KCl, 1.8 mM KH_2PO_4, 2 mM $CaCl_2$ [pH 7.4]) using wavelengths ranging from 195 nm to 250 nm, with 1-nm wavelength steps, in a 1-mm path length cell at 25°C. Temperature denaturation experiments were performed at a wavelength of 218 nm by increasing the temperature from 25°C to 100°C using a sealed cuvette, with 2°C temperature increments, 2 min temperature equilibration time, and 3 s averaging time.

Size Exclusion Multiangle Laser Light Scattering

SEC-MALS was performed using a WTC-030S5 column (Wyatt Technology) at a flow rate of 0.5 ml/min. Measurements were performed in PBS buffer. The elution profile was monitored by UV absorption at 280 nm, light scattering at 690 nm, and differential refractometry using Dawn Heleosand OptiLabrEX instruments (Wyatt Technology). Analyses were carried out using the Astra software. For each sample, 100 μl of C1QL3 protein at 3–17 mg/ml protein was loaded. A differential refractive index increment (d*n*/dc) value of 0.185 was used in the analysis of the SEC-MALS experiments.

Isothermal Calorimetry

Wild-type and mutant C1QL proteins were dialyzed against a buffer solution containing 10 mM HEPES (pH 7.4), 100 mM NaCl, and 5 mM EDTA overnight. The final dialysis buffer contained 10 mM HEPES (pH 7.4), 100 mM NaCl using UltraPure Water (Invitrogen, Thermo Fisher Scientific) to remove EDTA from solution. The final buffer was saved and used as washing buffer for the ITC instrument. The ITC experiments were carried out with a VP-ITC calorimeter (MicroCal, GE Healthcare). Samples were degassed for 10 min before the experiment. The wild-type or mutant C1QL protein solutions of 50 μM concentration were placed in the MicroCal sample cell. $CaCl_2$ solution with concentrations ranging from 5 to 0.625 mM was placed in a syringe. The $CaCl_2$ solutions were serially injected into the sample cell using 2-μl injections at 22°C. The ITC data were processed with a model treating all sites equivalent and fitted and deconvoluted using the ORIGIN software provided by MicroCal.

Crystallization and Diffraction Data Collection

Initial screens for crystallization of C1QL1, C1QL2, and C1QL3 were carried out using 96-well format kits (Hampton Index, Salt and Crystal Screen HT, Hampton Research) on a Phoenix crystallization robot (Art Robbins Instruments). Initial hits from the 96-well format were optimized using hanging drop in a 24-well format. Crystallization was performed at 19°C by the hanging-drop method. From 2 to 1.5 μl of protein sample was mixed with an equal volume of reservoir solution and equilibrated against 1 ml of reservoir solution. Crystals grew to sizes suitable for X-ray diffraction in 5 days to 2 weeks. Paraffin was used as a cryoprotectant. Excess paraffin was removed from the loop by dipping it on a cover slip surface and then immediately flash cooled in liquid nitrogen. Diffraction data were collected at the beamline BL 12-2, 11-1 of the Stanford Synchrotron Radiation Lightsource (SSRL) at SLAC National Accelerator Laboratory (C1QL1, C1QL3) and at beamline BL8.22 of the Advanced Light Source (ALS) at Lawrence Berkeley National Laboratory (C1QL2) (Table 1).

Structure Determination and Analysis

Diffraction data were processed, reduced, and scaled with XDS (Kabsch, 2010) or MOSFLM (Leslie and Powell, 2007) and AIMLESS (Evans, 2006). Initial phases were obtained by molecular replacement using a model that was generated by a sequence alignment of C1QL3 alignment with mouse adiponectin (PDB ID 1C3H, chain E) (Shapiro and Scherer, 1998) and modeling using Chainsaw (Stein, 2008), in which all nonconserved residues were mutated to alanine. Molecular replacement was performed with Phaser (McCoy et al., 2007) as implemented in the CCP4 software package (Winn et al., 2011). Iterative model building and refinement were carried out using Coot (Emsley et al., 2010) and phenix.refine (Adams et al., 2010), respectively (Table 1). All subsequent crystal structures were determined using C1QL3 as a model for molecular replacement.

The crystal structures of C1QL1 and C1QL2 contained a trimer in the asymmetric unit, whereas the crystal structures of C1QL3 at pH 4.3, C1QL3 D205A, and C1QL3 D207A contained a protomer in the asymmetric unit, and the biological trimer is generated by crystal symmetry. The crystal structure of C1QL3 at pH 6.5 contained three C1QL3 trimers in the asymmetric unit in space group P1. The crystallization condition of C1QL1, C1QL3 at pH 4.3, and C1QL3 D207A contained Cd^{2+}, whereas the condition of C1QL2 did not contain any divalent cations, and the conditions of C1QL3 at pH 6.5 and C1QL D205A contained Mg^{2+} (Table 1). The quality of the final models was analyzed by Molprobity (Chen et al., 2010).

Electrostatic Surface Potential Calculations

Electrostatic charges were calculated from the respective crystal structures, using the PARSE force field (Sitkoff et al., 1994; Tang et al., 2007) and setting pH to 7.5, as implemented in the server-based version of PDB2PQR (nbcr-222.ucsd.edu/pdb2pqr_1.8/) (Dolinsky et al., 2004). Bound metal ions were included in the calculations if they were present in the corresponding crystal structures. The resulting PQR file was used to calculate and display the electrostatic surface potential using the APBS (Baker et al., 2001) method implemented in PyMOL (DeLano, 2002).

Model Fitting and Figure Preparation

The model of the 18-mer oligomer of C1QL3 was docked into the EM density map of adiponectin using Chimera (Pettersen et al., 2004). Movies were created with Chimera (Pettersen et al., 2004) and PyMOL (DeLano, 2002) and edited in iMovie (Apple). Figures representing C1QL structures were prepared using PyMOL, and all graphs were prepared using Origin (OriginLab) and Adobe Illustrator (Adobe Systems).

ACCESSION NUMBERS

The final model and structural factors have been deposited in the PDB (http://www.pdb.org) under accession codes 4QQ2 (C1QL1), 4QPY (C1QL2), 4QQH (C1QL3 in space group H32), 4QQL (C1QL3 in space group P1), 4QQO (C1QL3 D205A), and 4QQP (C1QL3 D207A).

SUPPLEMENTAL INFORMATION

Supplemental Information includes five figures, one table, three movies, and 3D molecular models and can be found with this article online at http://dx.doi.org/10.1016/j.str.2015.01.019.

AUTHOR CONTRIBUTIONS

S.R. designed the research, performed experiments, and wrote the manuscript, B.K.V. performed experiments, S.V. suggested experiments and performed the initial SEC-MALS experiments and data analysis and reviewed the manuscript, D.C.M. provided helpful discussions and reviewed the manuscript, and T.C.S. and A.T.B. provided guidance and edited the manuscript.

ACKNOWLEDGMENTS

S.R. thanks Marc Bolliger for initial collaboration and helpful discussions, Prof. Alok K. Mitra for providing the adiponectin electron density map file, and Artem Lyubimov for helpful comments on the manuscript. Crystallographic data collection was carried out at the Stanford Synchrotron Radiation Lightsource (SSRL) and the Advanced Light Source (ALS) at the Lawrence Berkeley National Laboratory. The SSRL is a national user facility operated by Stanford University on behalf of the US Department of Energy, Office of Basic Energy Sciences. The SSRL Structural Molecular Biology Program is supported by the Department of Energy, Office of Biological and Environmental Research, and by the NIH, National Center for Research Resources, Biomedical Technology Program, and the National Institute of General Medical Sciences. We thank SSRL scientist Clyde Smith and TzankoDoukov for excellent support. The ALS is part of the Lawrence Berkeley Laboratory and operated by the US Department of Energy, Office of Basic Energy Science. We thank ASL scientist Corie Ralston for excellent support. S.R. held an EMBO Longterm fellowship and was an Otto-Hahn fellow of the Max-Planck Society Germany. D.C.M. holds a NIDA fellowship F32 DA031654.

Received: August 27, 2014
Revised: January 27, 2015
Accepted: January 28, 2015
Published: March 5, 2015

REFERENCES

Adams, P.D., Afonine, P.V., Bunkóczi, G., Chen, V.B., Davis, I.W., Echols, N., Headd, J.J., Hung, L.-W., Kapral, G.J., Grosse-Kunstleve, R.W., et al. (2010). PHENIX: a comprehensive Python-based system for macromolecular structure solution. Acta Crystallogr. D. Biol. Crystallogr. *66*, 213–221.

Bao, D., Pang, Z., and Morgan, J.I. (2005). The structure and proteolytic processing of Cbln1 complexes. J. Neurochem. *95*, 618–629.

Baker, N.A., Sept, D., Joseph, S., Holst, M.J., and McCammon, J.A. (2001). Electrostatics of nanosystems: application to microtubules and the ribosome. Proc. Natl. Acad. Sci. USA *98*, 10037–10041.

Bogin, O., Kvansakul, M., Rom, E., Singer, J., Yayon, A., and Hohenester, E. (2002). Insight into Schmid metaphyseal chondrodysplasia from the crystal structure of the collagen X NC1 domain trimer. Structure *10*, 165–173.

Bolliger, M.F., Martinelli, D.C., and Sudhof, T.C. (2011). The cell-adhesion G protein-coupled receptor BAI3 is a high-affinity receptor for C1q-like proteins. Proc. Natl. Acad. Sci. USA *108*, 2534–2539.

Boudko, S.P., Sasaki, T., Engel, J., Lerch, T.F., Nix, J., Chapman, M.S., and Bächinger, H.P. (2009). Crystal structure of human collagen XVIII trimerization domain: a novel collagen trimerization fold. J. Mol. Biol. *392*, 787–802.

Chen, V.B., Arendall, W.B., Headd, J.J., Keedy, D.A., Immormino, R.M., Kapral, G.J., Murray, L.W., Richardson, J.S., and Richardson, D.C. (2010). MolProbity: all-atom structure validation for macromolecular crystallography. Acta Crystallogr. D. Biol. Crystallogr. *66*, 12–21.

Cork, S.M., and Van Meir, E.G. (2011). Emerging roles for the BAI1 protein family in the regulation of phagocytosis, synaptogenesis, neurovasculature, and tumor development. J. Mol. Med. *89*, 743–752.

DeLano, W.L. (2002). The PyMOL Molecular Graphics System Version 1. (Schrödinger), available online at. http://www.pymol.org.

DeRosse, P., Lencz, T., Burdick, K.E., Siris, S.G., Kane, J.M., and Malhotra, A.K. (2008). The genetics of symptom-based phenotypes: toward a molecular classification of schizophrenia. Schizophr. Bull. *34*, 1047–1053.

Dolinsky, T.J., Nielsen, J.E., McCammon, J.A., and Baker, N.A. (2004). PDB2PQR: an automated pipeline for the setup of Poisson-Boltzmann electrostatics calculations. Nucleic Acids Res. *32*, W665–W667.

Emsley, P., Lohkamp, B., Scott, W.G., and Cowtan, K. (2010). Features and development of Coot. Acta Crystallogr. D. Biol. Crystallogr. *66*, 486–501.

Evans, P. (2006). Scaling and assessment of data quality. Acta Crystallogr. D. Biol. Crystallogr. *62*, 72–82.

Gaboriaud, C., Juanhuix, J., Gruez, A., Lacroix, M., Darnault, C., Pignol, D., Verger, D., Fontecilla-Camps, J.C., and Arlaud, G.J. (2003a). The crystal structure of the globular head of complement protein C1q provides a basis for its versatile recognition properties. J. Biol. Chem. *278*, 46974–46982.

Gaboriaud, C., Juanhuix, J., Gruez, A., Lacroix, M., Darnault, C., Pignol, D., Verger, D., Fontecilla-Camps, J.C., and Arlaud, G.J. (2003b). The crystal structure of the globular head of complement protein C1q provides a basis for its versatile recognition properties. J. Biol. Chem. *278*, 46974–46982.

Hamoud, N., Tran, V., Croteau, L.-P., Kania, A., and Côté, J.-F. (2014). G-protein coupled receptor BAI3 promotes myoblast fusion in vertebrates. Proc. Natl. Acad. Sci. USA *111*, 3745–3750.

Hirai, H., Pang, Z., Bao, D., Miyazaki, T., Li, L., Miura, E., Parris, J., Rong, Y., Watanabe, M., Yuzaki, M., et al. (2005). Cbln1 is essential for synaptic integrity and plasticity in the cerebellum. Nat. Neurosci. *8*, 1534–1541.

Hochreiter-Hufford, A.E., Lee, C.S., Kinchen, J.M., Sokolowski, J.D., Arandjelovic, S., Call, J.A., Klibanov, A.L., Yan, Z., Mandell, J.W., and Ravichandran, K.S. (2013). Phosphatidylserine receptor BAI1 and apoptotic cells as new promoters of myoblast fusion. Nature *497*, 263–267.

Hug, C., Wang, J., Ahmad, N.S., Bogan, J.S., Tsao, T.-S., and Lodish, H.F. (2004). T-cadherin is a receptor for hexameric and high-molecular-weight forms of Acrp30/adiponectin. Proc. Natl. Acad. Sci. USA *101*, 10308–10313.

Iijima, T., Miura, E., Watanabe, M., and Yuzaki, M. (2010). Distinct expression of C1q-like family mRNAs in mouse brain and biochemical characterization of their encoded proteins. Eur. J. Neurosci. *31*, 1606–1615.

Kabsch, W. (2010). XDS. Acta Crystallogr. D. Biol. Crystallogr. *66*, 125–132.

Kadowaki, T., and Yamauchi, T. (2005). Adiponectin and adiponectin receptors. Endocr. Rev. *26*, 439–451.

Kakegawa, W., Mitakidis, N., Miura, E., Abe, M., Matsuda, K., Takeo, Y.H., Kohda, K., Motohashi, J., Takahashi, A., Nagao, S., et al. (2015). Anterograde C1ql1 signaling is required in order to determine and maintain a single-winner climbing fiber in the mouse cerebellum. Neuron *85*, 316–329.

Kan, Z., Jaiswal, B.S., Stinson, J., Janakiraman, V., Bhatt, D., Stern, H.M., Yue, P., Haverty, P.M., Bourgon, R., Zheng, J., et al. (2010). Diverse somatic mutation patterns and pathway alterations in human cancers. Nature *466*, 869–873.

Kojouharova, M.S., Gadjeva, M.G., Tsacheva, I.G., Zlatarova, A., Roumenina, L.T., Tchorbadjieva, M.I., Atanasov, B.P., Waters, P., Urban, B.C., Sim, R.B., et al. (2004). Mutational analyses of the recombinant globular regions of human C1q A, B, and C chains suggest an essential role for arginine and histidine residues in the C1q-IgG interaction. J. Immunol. *172*, 4351–4358.

Krissinel, E., and Henrick, K. (2007). Inference of macromolecular assemblies from crystalline state. J. Mol. Biol. *372*, 774–797.

Kvansakul, M., Bogin, O., Hohenester, E., and Yayon, A. (2003). Crystal structure of the collagen α1(VIII) NC1 trimer. Matrix Biol. *22*, 145–152.

Leslie, A.G.W., and Powell, H.R. (2007). Processing diffraction data with mosflm. In Evolving Methods for Macromolecular Crystallography, *Vol. 245*, R.J. Read and J.L. Sussman, eds.. NATO Science Series II: Mathematics, Physics and Chemistry (Springer), 4151.

Liu, Q.-R., Drgon, T., Johnson, C., Walther, D., Hess, J., and Uhl, G.R. (2006). Addiction molecular genetics: 639,401 SNP whole genome association identifies many "cell adhesion" genes. Am. J. Med. Genet. B. Neuropsychiatr. Genet. *141B*, 918–925.

Matsuda, K., and Yuzaki, M. (2011). Cbln family proteins promote synapse formation by regulating distinct neurexin signaling pathways in various brain regions. Eur. J. Neurosci. *33*, 1447–1461.

Matsuda, K., Miura, E., Miyazaki, T., Kakegawa, W., Emi, K., Narumi, S., Fukazawa, Y., Ito-Ishida, A., Kondo, T., Shigemoto, R., et al. (2010). Cbln1 is

a ligand for an orphan glutamate receptor delta2, a bidirectional synapse organizer. Science *328*, 363–368.

McCoy, A.J., Grosse-Kunstleve, R.W., Adams, P.D., Winn, M.D., Storoni, L.C., and Read, R.J. (2007). Phaser crystallographic software. J. Appl. Crystallogr. *40*, 658–674.

Pettersen, E.F., Goddard, T.D., Huang, C.C., Couch, G.S., Greenblatt, D.M., Meng, E.C., and Ferrin, T.E. (2004). UCSF Chimera–a visualization system for exploratory research and analysis. J. Comput. Chem. *25*, 1605–1612.

Radjainia, M., Wang, Y., and Mitra, A.K. (2008). Structural polymorphism of oligomeric adiponectin visualized by electron microscopy. J. Mol. Biol. *381*, 419–430.

Reid, K.B., Gagnon, J., and Frampton, J. (1982). Completion of the amino acid sequences of the A and B chains of subcomponent C1q of the first component of human complement. Biochem. J. *203*, 559–569.

Roumenina, L.T., Kantardjiev, A.A., Atanasov, B.P., Waters, P., Gadjeva, M., Reid, K.B.M., Mantovani, A., Kishore, U., and Kojouharova, M.S. (2005). Role of Ca2+ in the electrostatic stability and the functional activity of the globular domain of human C1q. Biochemistry *44*, 14097–14109.

Rusakov, D.A., and Fine, A. (2003). Extracellular Ca2+ depletion contributes to fast activity-dependent modulation of synaptic transmission in the brain. Neuron *37*, 287–297.

Shapiro, L., and Scherer, P.E. (1998). The crystal structure of a complement-1q family protein suggests an evolutionary link to tumor necrosis factor. Curr. Biol. *8*, 335–338.

Sigoillot, S.M., Iyer, K., Binda, F., González-Calvo, I., Talleur, M., Vodjdani, G., Isope, P., and Selimi, F. (2015). The Secreted Protein C1QL1 and Its Receptor BAI3 Control the Synaptic Connectivity of Excitatory Inputs Converging on Cerebellar Purkinje Cells. CELL Reports *10*, 820–832.

Sitkoff, D., Sharp, K.A., and Honig, B. (1994). Accurate calculation of hydration free energies using macroscopic solvent models. J. Phys. Chem. *98*, 1978–1988.

Stein, N. (2008). A program for mutating PDB files used as templates in molecular replacement. J. Appl. Crystallogr. *41*, 641–643.

Stephenson, J.R., Purcell, R.H., and Hall, R.A. (2014). The BAI subfamily of adhesion GPCRs: synaptic regulation and beyond. Trends Pharmacol. Sci. *35*, 208–215.

Stevens, B., Allen, N.J., Vazquez, L.E., Howell, G.R., Christopherson, K.S., Nouri, N., Micheva, K.D., Mehalow, A.K., Huberman, A.D., Stafford, B., et al. (2007). The classical complement cascade mediates CNS synapse elimination. Cell *131*, 1164–1178.

Südhof, T.C. (2008). Neuroligins and neurexins link synaptic function to cognitive disease. Nature *455*, 903–911.

Tang, C.L., Alexov, E., Pyle, A.M., and Honig, B. (2007). Calculation of pKas in RNA: on the structural origins and functional roles of protonated nucleotides. J. Mol. Biol. *366*, 1475–1496.

Tsao, T.-S., Tomas, E., Murrey, H.E., Hug, C., Lee, D.H., Ruderman, N.B., Heuser, J.E., and Lodish, H.F. (2003). Role of disulfide bonds in Acrp30/adiponectin structure and signaling specificity. Different oligomers activate different signal transduction pathways. J. Biol. Chem. *278*, 50810–50817.

Tu, X., and Palczewski, K. (2012). Crystal structure of the globular domain of C1QTNF5: implications for late-onset retinal macular degeneration. J. Struct. Biol. *180*, 439–446.

Uemura, T., Lee, S.J., Yasumura, M., Takeuchi, T., Yoshida, T., Ra, M., Taguchi, R., Sakimura, K., and Mishina, M. (2010). Trans-synaptic interaction of GluRdelta2 and neurexin through Cbln1 mediates synapse formation in the cerebellum. Cell *141*, 1068–1079.

Unni, S., Huang, Y., Hanson, R.M., Tobias, M., Krishnan, S., Li, W.W., Nielsen, J.E., and Baker, N.A. (2011). Web servers and services for electrostatics calculations with APBS and PDB2PQR. J. Comput. Chem. *32*, 1488–1491.

Waki, H., Yamauchi, T., Kamon, J., Ito, Y., Uchida, S., Kita, S., Hara, K., Hada, Y., Vasseur, F., Froguel, P., et al. (2003). Impaired multimerization of human adiponectin mutants associated with diabetes. Molecular structure and multimer formation of adiponectin. J. Biol. Chem. *278*, 40352–40363.

Winn, M.D., Ballard, C.C., Cowtan, K.D., Dodson, E.J., Emsley, P., Evans, P.R., Keegan, R.M., Krissinel, E.B., Leslie, A.G.W., McCoy, A., et al. (2011). Overview of the CCP4 suite and current developments. Acta Crystallogr. D. Biol. Crystallogr. *67*, 235–242.

Wirz, J.A., Boudko, S.P., Lerch, T.F., Chapman, M.S., and Bächinger, H.P. (2011). Crystal structure of the human collagen XV trimerization domain: a potent trimerizing unit common to multiplexin collagens. Matrix Biol. *30*, 9–15.

Yamauchi, T., Kamon, J., Waki, H., Imai, Y., Shimozawa, N., Hioki, K., Uchida, S., Ito, Y., Takakuwa, K., Matsui, J., et al. (2003). Globular adiponectin protected ob/ob mice from diabetes and ApoE-deficient mice from atherosclerosis. J. Biol. Chem. *278*, 2461–2468.

Zheng, H., Chordia, M.D., Cooper, D.R., Chruszcz, M., Müller, P., Sheldrick, G.M., and Minor, W. (2014). Validation of metal-binding sites in macromolecular structures with the CheckMyMetal web server. Nat. Protoc. *9*, 156–170.